Pramana – J. Phys. (2019) 93:6
https://doi.org/10.1007/s12043-019-1763-x

A new efficient technique for solving fractional coupled Navier–Stokes equations using q-homotopy analysis transform method

AMIT PRAKASH[1], P VEERESHA[2], D G PRAKASHA[2],* and MANISH GOYAL[3]

[1]Department of Mathematics, National Institute of Technology, Kurukshetra 136 119, India
[2]Department of Mathematics, Karnataka University, Dharwad 580 003, India
[3]Department of Mathematics, IAH, GLA University, Mathura 281 406, India
*Corresponding author. E-mail: prakashadg@gmail.com; dgprakasha@kud.ac.in

MS received 13 July 2018; revised 6 December 2018; accepted 13 December 2018;
published online 30 April 2019

Abstract. In this paper, a solution of coupled fractional Navier–Stokes equation is computed numerically using the proposed q-homotopy analysis transform method (q-HATM), and the solution is found in fast convergent series. The given test examples illustrate the leverage and effectiveness of the proposed technique. The obtained results are demonstrated graphically. The present method handles the series solution in a large admissible domain in an extreme manner. It offers us a modest way to adjust the convergence region of the solution. Results with graphs explicitly reveal the efficiency and capability of the proposed algorithm.

Keywords. Navier–Stokes equations; q-homotopy analysis transform method; Caputo fractional derivative; Laplace transform; homotopy analysis method.

PACS Nos 02.60.–Cb; 05.45.–a

1. Introduction

A fraction in derivative was concieved by Leibnitz and it was revealed that fractional calculus is more suitable for modelling real-world problems than classical calculus. The theory of fractional calculus interprets the reality of nature in an excellent and systematic manner [1–3]. Recently, it has garnered attention as it can deliver exact explanation regarding nonlinear complex systems. Fractional-order derivative has gained more attention in various areas, e.g. fluid dynamics [4], electrodynamics [5], nanotechnology, finance, neurophysiology [6], etc. Differential equations that govern systems with memory are fractional differential equations (FDEs) [7–9]. Arbitrariness in their order introduces more degrees of freedom in design and analysis, resulting in more accurate modelling, better robustness in control and greater flexibility in signal processing. Electrochemical phenomena such as double-layer charge distribution or diffusion process can be better explained with a fractional-order system. As a result, the modelling of lithium in batteries, fuel cells and supercapacitors is carried out with FDEs. Other promising areas of applications include the characterisation of ceramic bodies, fractal structures, viscoelastic materials, and decay rate of fruit and meat and the study of corrosion in a metal surface.

The advantage of using fractional models of differential equations in physical models is their non-local property. Fractional-order derivative is non-local, whereas integer-order derivative is local in nature. It shows that the upcoming state of the physical system is also dependent on all of its historical states in addition to its present state. Hence, fractional models are more realistic [10,11].

In 1822, Navier derived the Navier–Stokes (NS) equation, which portrays the flow motion of a viscous fluid. As examples of the motion of a fluid, they described various physical phenomena, e.g. blood flow, ocean current, flow of liquid in pipes and air flow around the arms of an aircraft. Its exact solution is possible in only a few cases due to its nonlinear nature. In these cases, we have to consider a simple configuration for the flow pattern and certain assumptions need to be made about the state of the fluid. In most practical situations, these equations follow the fractional order and not the integer order. El-Shahed and Salam [12] generalised the classical NS equation by switching integer-order derivative to arbitrary-order derivative α $(0 < \alpha \leq 1)$. Many

methods are available in the literature to solve fractional-order NS equations. For more details, we direct readers to papers [13–15] and references therein.

In this work, we consider a time-fractional NS equation for an incompressible fluid flow of density ρ and kinematic viscosity $\nu = \eta/\rho$. It is given as

$$\begin{cases} D_t^\alpha U + (U \cdot \nabla)U = \rho_0 \nabla^2 U - \dfrac{1}{\rho}\nabla p, \\ \nabla \cdot U = 0, \\ U = 0, \text{ on } \Omega \times (0, T). \end{cases} \tag{1}$$

Here, $U = (u, v, w)$, p and t denote fluid vector, pressure and time, respectively. (x, y, z) represent the spatial components in Ω. η is the dynamic viscosity. ρ is the density and the ratio of η and ρ is ρ_0.

Equation (1) can also be represented as

$$\begin{cases} D_t^\alpha u + u\dfrac{\partial u}{\partial x} + v\dfrac{\partial u}{\partial y} + w\dfrac{\partial u}{\partial z} \\ \quad = \rho_0\left(\dfrac{\partial^2 u}{\partial x^2} + \dfrac{\partial^2 u}{\partial y^2} + \dfrac{\partial^2 u}{\partial z^2}\right) - \dfrac{1}{\rho}\dfrac{\partial p}{\partial x}, \\ D_t^\alpha v + u\dfrac{\partial v}{\partial x} + v\dfrac{\partial v}{\partial y} + w\dfrac{\partial v}{\partial z} \\ \quad = \rho_0\left(\dfrac{\partial^2 v}{\partial x^2} + \dfrac{\partial^2 v}{\partial y^2} + \dfrac{\partial^2 v}{\partial z^2}\right) - \dfrac{1}{\rho}\dfrac{\partial p}{\partial x}, \\ D_t^\alpha w + u\dfrac{\partial w}{\partial x} + v\dfrac{\partial w}{\partial y} + w\dfrac{\partial w}{\partial z} \\ \quad = \rho_0\left(\dfrac{\partial^2 w}{\partial x^2} + \dfrac{\partial^2 w}{\partial y^2} + \dfrac{\partial^2 w}{\partial z^2}\right) - \dfrac{1}{\rho}\dfrac{\partial p}{\partial x}, \end{cases} \tag{2}$$

Fractional derivative is taken in Caputo sense. The aim is to propose an efficient scheme for fractional-order NS equations. Liao [16] presented the homotopy analysis method (HAM) in which an incessant mapping is formed from initial speculation to an exact solution after selecting an auxiliary linear operator. The solution convergence is confirmed by the auxiliary parameter. The q-HAM is actually an improvement of $q \in [0, 1]$ in HAM to $q \in [0, 1/n], n \geq 1$. The presence of the term $(1/n)^m$ in the solution gives faster convergence than the standard HAM. The combination of semianalytical methods with a suitable transform reduces the time consumption in investigating solutions to nonlinear problems describing real-life applications. The q-homotopy analysis transform method (q-HATM) [17–20] is an amalgamation of q-HAM and transform of Laplace. Its superiority is its ability to adjust two strong computational methodologies for probing FDEs. By choosing proper $\hbar$, we can control the convergence region of solution series in a large permissible domain.

A fraction in the time derivative recommends modulation of system memory. Time-FDEs describe the motion of a particle with memory in time. It is apparent that viscous fluid flow is influenced by memory. This means that fractional modelling is suitable for such systems. Hence, the study of time-fractional NS equations is very important. The time-fractional NS equations have not yet been studied by q-HATM. Finding their numerical solution by q-HATM seems interesting due to the qualities of q-HATM in that it does not require linearisation or discretisation, shows little perturbations, has no restrictive assumptions, lessens mathematical computations significantly, offers non-local effect, promises a big convergence region and is free from obtaining difficult polynomials, integrations and physical parameters.

This paper is structured in the following manner. Section 1 is the introduction. In §2, we give a brief review of the preliminary description of Caputo's fractional derivative and its transform. In §3, the basic plan of the proposed numerical method q-HATM is shown. In §4, some trial examples are offered to show the efficiency of the projected technique. Section 5 deals with the discussion of the obtained numerical results and their significance. Figures are drawn using the Maple package. Finally, in §6, we recapitulate our outcomes and draw inferences.

2. Preliminaries

DEFINITION 1

Caputo fractional order derivative [7] of $f(t)$, $f \in C_\beta$, $\beta \geq -1$, is

$$D_t^\alpha f(t) = \begin{cases} \dfrac{\mathrm{d}^n f(t)}{\mathrm{d}t^n}, & \alpha = n \in \mathbb{N}, \\ \dfrac{1}{\Gamma(n-\alpha)}\displaystyle\int_0^t (t-\vartheta)^{n-\alpha-1} f^n(\vartheta)\,\mathrm{d}\vartheta, \\ n-1 < \alpha < n, \quad n \in \mathbb{N}. \end{cases} \tag{3}$$

DEFINITION 2

Laplace transform [7] of $D_t^\alpha f(t)$ is

$$L\left[D_t^\alpha f(t)\right] = s^\alpha F(s) - \sum_{r=0}^{n-1} s^{\alpha-r-1} f^{(r)}(0^+), \quad (n-1 < \alpha \leq n). \tag{4}$$

3. Suggested new q-homotopy analysis transform method

Consider a non-homogeneous and nonlinear fractional-order PDE:

$$D_t^\alpha \mathcal{U}(x, y, t) + R\mathcal{U}(x, y, t) + N\mathcal{U}(x, y, t) = f(x, y, t), \quad n-1 < \alpha \leq n. \tag{5}$$

Here, $D_t^\alpha \mathcal{U}$ is the Caputo derivative and R and N are linear and nonlinear operators, respectively. $f(x, y, t)$ is the source term.

Now, employing the transform of Laplace on eq. (5) and solving, we find

$$L[\mathcal{U}(x, y, t)] - \frac{1}{s^\alpha}\sum_{k=0}^{n-1} s^{\alpha-k-1}\,\mathcal{U}^k(x, y, 0) + \frac{1}{s^\alpha}\{L[R\mathcal{U}(x, y, t)] + L[N\mathcal{U}(x, y, t)] - L[f(x, y, t)]\} = 0. \tag{6}$$

The nonlinear operator is

$$N[\varphi(x, y, t; q)] = L[\varphi(x, y, t; q)] - \frac{1}{s^\alpha}\sum_{k=0}^{n-1} s^{\alpha-k-1}\,\varphi^{(k)}(x, y, t; q)\big(0^+\big) + \frac{1}{s^\alpha}\{L[R\varphi(x, y, t; q)] + L[N\varphi(x, y, t; q)] - L[f(x, y, t)]\}. \tag{7}$$

Here, $q \in \left[0, \frac{1}{n}\right]$ is the embedding parameter, $n \geq 1$ and $\varphi(x, y, t; q)$ is an unknown function.

Construct a homotopy as

$$(1 - nq)L[\varphi(x, y, t; q) - \mathcal{U}_0(x, y, t)] = hqH(x, y, t)N[\varphi(x, y, t; q)], \tag{8}$$

where $\hbar \neq 0$ is an auxiliary parameter and $\mathcal{U}_0$ is an initial guess.

The following results hold for $= 0, \frac{1}{n}$:

$$\varphi(x, y, t; 0) = \mathcal{U}_0(x, y, t),$$
$$\varphi\left(x, y, t; \frac{1}{n}\right) = \mathcal{U}(x, y, t). \tag{9}$$

By amplifying q, φ converges from $\mathcal{U}_0$ to $\mathcal{U}$.

Escalating φ about q by Taylor's theorem, we have

$$\varphi(x, y, t; q) = \mathcal{U}_0 + \sum_{m=1}^{\infty} \mathcal{U}_m(x, y, t)q^m, \tag{10}$$

where

$$\mathcal{U}_m = \frac{1}{m!}\frac{\partial^m \varphi(x, y, t; q)}{\partial q^m}\bigg|_{q=0}. \tag{11}$$

By a proper choice of auxiliary linear operator, $\mathcal{U}_0$, n, $\hbar$ and H, series (10) converges at $q = 1/n$, thereby giving a solution

$$\mathcal{U}(x, y, t) = \mathcal{U}_0 + \sum_{m=1}^{\infty} \mathcal{U}_m(x, y, t)\left(\frac{1}{n}\right)^m. \tag{12}$$

Now, differentiating eq. (8) m times, dividing by $m!$ and taking $q = 0$,

$$L\big[\mathcal{U}_m(x, y, t) - k_m\mathcal{U}_{m-1}\big(x, y, t\big)\big] = \hbar H(x, y, t)\Re_m\big(\vec{\mathcal{U}}_{m-1}\big), \tag{13}$$

where the vectors are defined as

$$\vec{\mathcal{U}}_m = \{\mathcal{U}_0(x, y, t), \mathcal{U}_1(x, y, t), \ldots, \mathcal{U}_m(x, y, t)\}. \tag{14}$$

Applying the inverse transform on eq. (13),

$$\mathcal{U}_m(x, y, t) = k_m\mathcal{U}_{m-1}(x, y, t) + \hbar L^{-1}\big[H(x, y, t)\Re_m\big(\vec{\mathcal{U}}_{m-1}\big)\big]. \tag{15}$$

Here,

$$\Re_m\big(\vec{\mathcal{U}}_{m-1}\big) = \frac{1}{(m-1)!}\frac{\partial^{m-1}N[\varphi(x, y, t; q)]}{\partial q^{m-1}}\bigg|_{q=0} \tag{16}$$

and

$$k_r = \begin{cases} 0, & r \leq 1, \\ n, & r > 1. \end{cases} \tag{17}$$

Finally, by solving eq. (15), the components of the q-HATM solution can be easily obtained.

4. Numerical experiments

Now, consider two test examples to illustrate the efficiency and applicability of the proposed technique.

Example 1. Consider a two-dimensional incompressible time-fractional NS equation [13,14]

$$\begin{cases} D_t^\alpha u + u\dfrac{\partial u}{\partial x} + v\dfrac{\partial u}{\partial y} = \rho_0\left(\dfrac{\partial^2 u}{\partial x^2} + \dfrac{\partial^2 u}{\partial y^2}\right) + g, \\ D_t^\alpha v + u\dfrac{\partial v}{\partial x} + v\dfrac{\partial v}{\partial y} = \rho_0\left(\dfrac{\partial^2 v}{\partial x^2} + \dfrac{\partial^2 v}{\partial y^2}\right) - g, \end{cases} \quad 0 < \alpha \leq 1 \tag{18}$$

and its initial settings

$$v(x, y, 0) = \sin(x + y),$$
$$u(x, y, 0) = -\sin(x + y). \tag{19}$$

Taking the Laplace transform on eq. (18) and using eq. (19), we get

$$L[u(x, y, t)] + \frac{\sin(x + y)}{s} + \frac{1}{s^\alpha}L\left\{u\frac{\partial u}{\partial x} + v\frac{\partial u}{\partial y} - \rho_0\left(\frac{\partial^2 u}{\partial x^2} + \frac{\partial^2 u}{\partial y^2}\right) - g\right\} = 0$$
$$L[v(x, y, t)] - \frac{\sin(x + y)}{s} + \frac{1}{s^\alpha}L\left\{u\frac{\partial v}{\partial x} + v\frac{\partial v}{\partial y}\right.$$

$$-\rho_0\left(\frac{\partial^2 v}{\partial x^2}+\frac{\partial^2 v}{\partial y^2}\right)+g\Big\}=0. \tag{20}$$

Define the nonlinear operators:

$$\begin{aligned}
&N^1[\varphi_1(x,y,t;q),\varphi_2(x,y,t;q)]\\
&\quad=L[\varphi_1(x,y,t;q)]+\frac{\sin(x+y)}{s}\\
&\qquad+\frac{1}{s^\alpha}L\Big\{\varphi_1(x,y,t;q)\frac{\partial\varphi_1(x,y,t;q)}{\partial x}\\
&\qquad+\varphi_2(x,y,t;q)\frac{\partial\varphi_1(x,y,t;q)}{\partial y}\\
&\qquad-\rho_0\Big(\frac{\partial^2\varphi_1(x,y,t;q)}{\partial x^2}\\
&\qquad+\frac{\partial^2\varphi_1(x,y,t;q)}{\partial y^2}\Big)-g\Big\},
\end{aligned} \tag{21}$$

$$\begin{aligned}
&N^2[\varphi_1(x,y,t;q),\varphi_2(x,y,t;q)]\\
&\quad=L[\varphi_2(x,y,t;q)]-\frac{\sin(x+y)}{s}\\
&\qquad+\frac{1}{s^\alpha}L\Big\{\varphi_1(x,y,t;q)\frac{\partial\varphi_2(x,y,t;q)}{\partial x}\\
&\qquad+\varphi_2(x,y,t;q)\frac{\partial\varphi_2(x,y,t;q)}{\partial y}\\
&\qquad-\rho_0\Big(\frac{\partial^2\varphi_2(x,y,t;q)}{\partial x^2}\\
&\qquad+\frac{\partial^2\varphi_2(x,y,t;q)}{\partial y^2}\Big)+g\Big\}
\end{aligned} \tag{22}$$

and the Laplace operators as

$$\begin{aligned}
&L\big[u_m(x,y,t)-k_m u_{m-1}(x,y,t)\big]\\
&\quad=\hbar R_{1,m}\big[\vec{u}_{m-1},\vec{v}_{m-1}\big],\\
&L\big[v_m(x,y,t)-k_m v_{m-1}(x,y,t)\big]\\
&\quad=\hbar R_{2,m}\big[\vec{u}_{m-1},\vec{v}_{m-1}\big].
\end{aligned} \tag{23}$$

Here,

$$\begin{aligned}
&R_{1,m}\big[\vec{u}_{m-1},\vec{v}_{m-1}\big]=L\big[u_{m-1}(x,y,t)\big]\\
&\qquad+\left(1-\frac{k_m}{n}\right)\frac{\sin(x+y)}{s}\\
&\qquad+\frac{1}{s^\alpha}L\Big\{\sum_{i=0}^{m-1}u_i\frac{\partial u_{m-1-i}}{\partial x}\\
&\qquad+\sum_{i=0}^{m-1}v_i\frac{\partial u_{m-1-i}}{\partial y}\\
&\qquad-\rho_0\Big(\frac{\partial^2 u_{m-1}}{\partial x^2}+\frac{\partial^2 u_{m-1}}{\partial y^2}\Big)-g\Big\},\\
&R_{2,m}\big[\vec{u}_{m-1},\vec{v}_{m-1}\big]=L\big[v_{m-1}(x,y,t)\big]\\
&\qquad-\left(1-\frac{k_m}{n}\right)\frac{\sin(x+y)}{s}\\
&\qquad+\frac{1}{s^\alpha}L\Big\{\sum_{i=0}^{m-1}u_i\frac{\partial v_{m-1-i}}{\partial x}\\
&\qquad+\sum_{i=0}^{m-1}v_i\frac{\partial v_{m-1-i}}{\partial y}\\
&\qquad-\rho_0\Big(\frac{\partial^2 v_{m-1}}{\partial x^2}+\frac{\partial^2 v_{m-1}}{\partial y^2}\Big)+g\Big\}.
\end{aligned} \tag{24}$$

Applying the inverse transform on eq. (23), we get

$$\begin{aligned}
u_m(x,y,t)&=k_m u_{m-1}\\
&\quad+\hbar L^{-1}\big\{R_{1,m}\big[\vec{u}_{m-1},\vec{v}_{m-1}\big]\big\},\\
v_m(x,y,t)&=k_m v_{m-1}\\
&\quad+\hbar L^{-1}\big\{R_{2,m}\big[\vec{u}_{m-1},\vec{v}_{m-1}\big]\big\}.
\end{aligned} \tag{25}$$

Using u_0 and v_0 in eq. (25), we get

$$\begin{aligned}
u_1&=-\frac{2\rho_0\hbar\sin(x+y)t^\alpha}{\Gamma[\alpha+1]},\\
v_1&=\frac{2\rho_0\hbar\sin(x+y)t^\alpha}{\Gamma[\alpha+1]},\\
u_2&=-\frac{2(n+\hbar)\rho_0\hbar\sin(x+y)t^\alpha}{\Gamma[\alpha+1]}\\
&\quad-\frac{4\rho_0^2\hbar^2\sin(x+y)t^{2\alpha}}{\Gamma[2\alpha+1]},\\
v_2&=\frac{2(n+\hbar)\rho_0\hbar\sin(x+y)t^\alpha}{\Gamma[\alpha+1]}\\
&\quad+\frac{4\rho_0^2\hbar^2\sin(x+y)t^{2\alpha}}{\Gamma[2\alpha+1]},\\
u_3&=-\frac{2(n+\hbar)^2\rho_0\hbar\sin(x+y)t^\alpha}{\Gamma[\alpha+1]}\\
&\quad-\frac{8(n+\hbar)\rho_0^2\hbar^2\sin(x+y)t^{2\alpha}}{\Gamma[2\alpha+1]}\\
&\quad-\frac{8\rho_0^3\hbar^3\sin(x+y)t^{3\alpha}}{\Gamma[3\alpha+1]},\\
v_3&=\frac{2(n+\hbar)^2\rho_0\hbar\sin(x+y)t^\alpha}{\Gamma[\alpha+1]}\\
&\quad+\frac{8(n+\hbar)\rho_0^2\hbar^2\sin(x+y)t^{2\alpha}}{\Gamma[2\alpha+1]}\\
&\quad+\frac{8\rho_0^3\hbar^3\sin(x+y)t^{3\alpha}}{\Gamma[3\alpha+1]}
\end{aligned}$$

and so on.

Similarly, the rest of the constituents are found. Then, the q-HATM solution of eq. (18) is obtained as

$$u(x, y, t) = u_0 + \sum_{m=1}^{\infty} u_m \left(\frac{1}{n}\right)^m,$$
$$v(x, y, t) = v_0 + \sum_{m=1}^{\infty} v_m \left(\frac{1}{n}\right)^m. \tag{26}$$

For $\alpha = 1, \hbar = -1$, $n = 1$ and $g = 0$, solutions $\sum_{m=1}^{N} u_m(x, y, t)(1/n)^m$ and $\sum_{m=1}^{N} v_m(x, y, t)(1/n)^m$ converge to exact results as $N \to \infty$:

$$\begin{aligned} u(x, y, t) &= -\sin(x + y)\left[1 - \frac{2\rho_0 t}{1!} + \frac{(2\rho_0 t)^2}{2!} - \frac{(2\rho_0 t)^3}{3!} + \cdots\right] \\ &= -\mathrm{e}^{-2\rho_0 t}\sin(x + y), \\ v(x, y, t) &= \sin(x + y)\left[1 - \frac{2\rho_0 t}{1!} + \frac{(2\rho_0 t)^2}{2!} - \frac{(2\rho_0 t)^3}{3!} + \cdots\right] \\ &= \mathrm{e}^{-2\rho_0 t}\sin(x + y). \end{aligned}$$

Example 2. In eq. (18), we take

$$v(x, y, 0) = \mathrm{e}^{x+y}, \quad u(x, y, 0) = -\mathrm{e}^{x+y}. \tag{27}$$

Taking the Laplace transform on eq. (18) and using eq. (27), we get

$$\begin{aligned} &L[u] + \frac{\mathrm{e}^{x+y}}{s} + \frac{1}{s^\alpha} L\left\{u\frac{\partial u}{\partial x} + v\frac{\partial u}{\partial y} - \rho_0\left(\frac{\partial^2 u}{\partial x^2} + \frac{\partial^2 u}{\partial y^2}\right) - g\right\} = 0, \\ &L[v] - \frac{\mathrm{e}^{x+y}}{s} + \frac{1}{s^\alpha} L\left\{u\frac{\partial v}{\partial x} + v\frac{\partial v}{\partial y} - \rho_0\left(\frac{\partial^2 v}{\partial x^2} + \frac{\partial^2 v}{\partial y^2}\right) + g\right\} = 0. \end{aligned} \tag{28}$$

Define nonlinear operators as

$$\begin{aligned} N^1[\varphi_1, \varphi_2] &= L[\varphi_1] + \frac{\mathrm{e}^{x+y}}{s} + \frac{1}{s^\alpha} L\left\{\varphi_1\frac{\partial \varphi_1}{\partial x} + \varphi_2\frac{\partial \varphi_1}{\partial y} - \rho_0\left(\frac{\partial^2 \varphi_1}{\partial x^2} + \frac{\partial^2 \varphi_1}{\partial y^2}\right) - g\right\}, \\ N^2[\varphi_1, \varphi_2] &= L[\varphi_2] - \frac{\mathrm{e}^{x+y}}{s} + \frac{1}{s^\alpha} L\left\{\varphi_1\frac{\partial \varphi_2}{\partial x} + \varphi_2\frac{\partial \varphi_2}{\partial y} - \rho_0\left(\frac{\partial^2 \varphi_2}{\partial x^2} + \frac{\partial^2 \varphi_2}{\partial y^2}\right) + g\right\} \end{aligned} \tag{29}$$

and Laplace operators as

$$\begin{aligned} &L\big[u_m(x, y, t) - k_m u_{m-1}(x, y, t)\big] = \hbar R_{1,m}\big[\vec{u}_{m-1}, \vec{v}_{m-1}\big], \\ &L\big[v_m(x, y, t) - k_m v_{m-1}(x, y, t)\big] = \hbar R_{2,m}\big[\vec{u}_{m-1}, \vec{v}_{m-1}\big] \end{aligned} \tag{30}$$

where

$$\begin{aligned} R_{1,m}\big[\vec{u}_{m-1}, \vec{v}_{m-1}\big] &= L\big[u_{m-1}\big] + \left(1 - \frac{k_m}{n}\right)\frac{\mathrm{e}^{x+y}}{s} + \frac{1}{s^\alpha} L\left\{\sum_{i=0}^{m-1} u_i \frac{\partial u_{m-1-i}}{\partial x} + \sum_{i=0}^{m-1} v_i \frac{\partial u_{m-1-i}}{\partial y} - \rho_0\left(\frac{\partial^2 u_{m-1}}{\partial x^2} + \frac{\partial^2 u_{m-1}}{\partial y^2}\right) - g\right\}, \\ R_{2,m}\big[\vec{u}_{m-1}, \vec{v}_{m-1}\big] &= L\big[v_{m-1}\big] - \left(1 - \frac{k_m}{n}\right)\frac{\mathrm{e}^{x+y}}{s} + \frac{1}{s^\alpha} L\left\{\sum_{i=0}^{m-1} u_i \frac{\partial v_{m-1-i}}{\partial x} + \sum_{i=0}^{m-1} v_i \frac{\partial v_{m-1-i}}{\partial y} - \rho_0\left(\frac{\partial^2 v_{m-1}}{\partial x^2} + \frac{\partial^2 v_{m-1}}{\partial y^2}\right) + g\right\}. \end{aligned} \tag{32}$$

By the inverse transform on eq. (31), we find

$$\begin{aligned} u_m(x, y, t) &= k_m u_{m-1} + \hbar L^{-1}\big\{R_{1,m}\big[\vec{u}_{m-1}, \vec{v}_{m-1}\big]\big\}, \\ v_m(x, y, t) &= k_m v_{m-1} + \hbar L^{-1}\big\{R_{2,m}\big[\vec{u}_{m-1}, \vec{v}_{m-1}\big]\big\}. \end{aligned} \tag{33}$$

Using u_0 and v_0, we get from eq. (33),

$$\begin{aligned} u_1 &= \frac{2\rho_0\hbar\mathrm{e}^{x+y}t^\alpha}{\Gamma[\alpha + 1]}, \qquad v_1 = -\frac{2\rho_0\hbar\mathrm{e}^{x+y}t^\alpha}{\Gamma[\alpha + 1]}, \\ u_2 &= \frac{2(n + \hbar)\rho_0\hbar\mathrm{e}^{x+y}t^\alpha}{\Gamma[\alpha + 1]} - \frac{4\rho_0^2\hbar^2\mathrm{e}^{x+y}t^{2\alpha}}{\Gamma[2\alpha + 1]}, \\ v_2 &= -\frac{2(n + \hbar)\rho_0\hbar\mathrm{e}^{x+y}t^\alpha}{\Gamma[\alpha + 1]} + \frac{4\rho_0^2\hbar^2\mathrm{e}^{x+y}t^{2\alpha}}{\Gamma[2\alpha + 1]}, \\ u_3 &= \frac{2(n + \hbar)^2\rho_0\hbar\mathrm{e}^{x+y}t^\alpha}{\Gamma[\alpha + 1]} - \frac{8(n + \hbar)\rho_0^2\hbar^2\mathrm{e}^{x+y}t^{2\alpha}}{\Gamma[2\alpha + 1]} \end{aligned}$$

$$+\frac{8\rho_0^3\hbar^3 e^{x+y}t^{3\alpha}}{\Gamma[3\alpha+1]},$$

$$v_3 = -\frac{2(n+\hbar)^2\rho_0\hbar e^{x+y}t^{\alpha}}{\Gamma[\alpha+1]} + \frac{8(n+\hbar)\rho_0^2\hbar^2 e^{x+y}t^{2\alpha}}{\Gamma[2\alpha+1]} - \frac{8\rho_0^3\hbar^3 e^{x+y}t^{3\alpha}}{\Gamma[3\alpha+1]}$$

and so on.

Similarly, rest of the constituents are found. The q-HATM solution of eq. (18) is

$$u(x,y,t) = u_0 + \sum_{m=1}^{\infty} u_m\left(\frac{1}{n}\right)^m,$$
$$v(x,y,t) = v_0 + \sum_{m=1}^{\infty} v_m\left(\frac{1}{n}\right)^m. \quad (34)$$

For $\alpha = 1 = n, \hbar = -1$ and $g = 0$, solutions $\sum_{m=1}^{N} u_m(1/n)^m$ and $\sum_{m=1}^{N} v_m(1/n)^m$ converge to exact solutions as $N \to \infty$.

$$u(x,y,t) = -e^{x+y}\left[1 + \frac{2\rho_0 t}{1!} + \frac{(2\rho_0 t)^2}{2!} + \frac{(2\rho_0 t)^3}{3!} + \cdots\right] = -e^{x+y+2\rho_0 t},$$

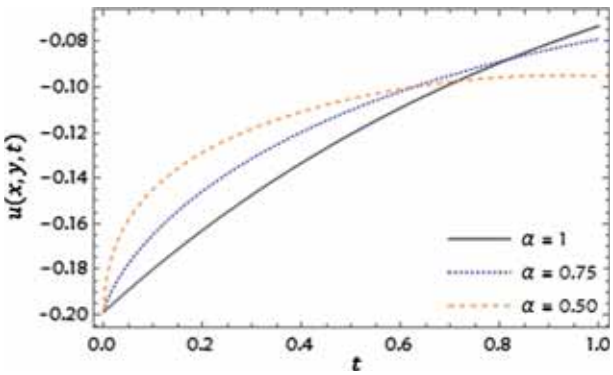

Figure 3. Plot of q-HATM solution $u(x, y, t)$ vs. t when $n = 1, \hbar = -1, g = 0, \rho_0 = 0.5$ and $x = 0.1 = y$ with diverse values of α, for Example 1.

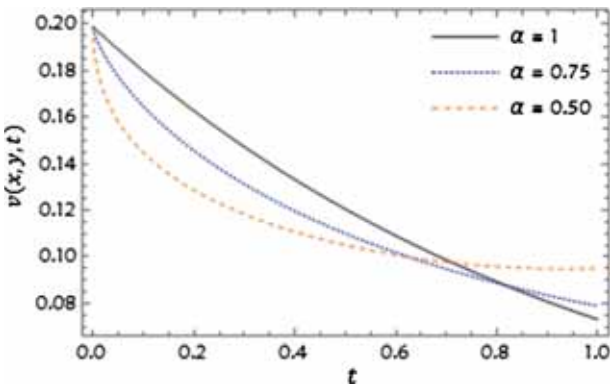

Figure 4. Plot of q-HATM solution $v(x, y, t)$ vs. t when $n = 1, \hbar = -1, g = 0, \rho_0 = 0.5$ and $x = 0.1 = y$ with diverse values of α, for Example 1.

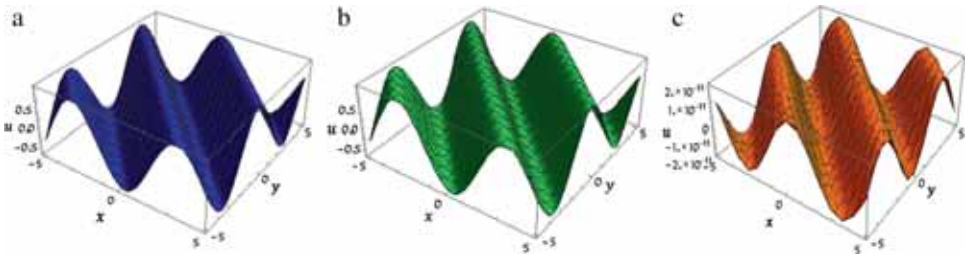

Figure 1. Surfaces of **(a)** approximate solution, **(b)** exact solution and **(c)** abs. error $= \left|u_{\text{exact}} - u_{\text{approx.}}\right|$ when $n = 1 = \alpha, \hbar = -1, g = 0, \rho_0 = 0.5$ and $t = 0.1$ for Example 1.

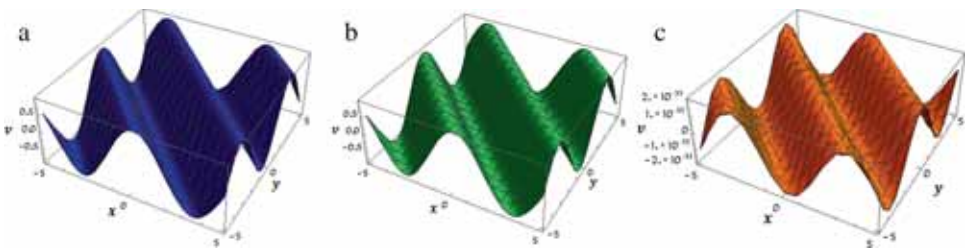

Figure 2. Surfaces of (**a**) approximate solution, (**b**) exact solution and (**c**) abs. error $= \left|v_{\text{exact}} - v_{\text{approx.}}\right|$ when $n = 1 = \alpha, \hbar = -1, g = 0, \rho_0 = 0.5$ and $t = 0.1$ for Example 1.

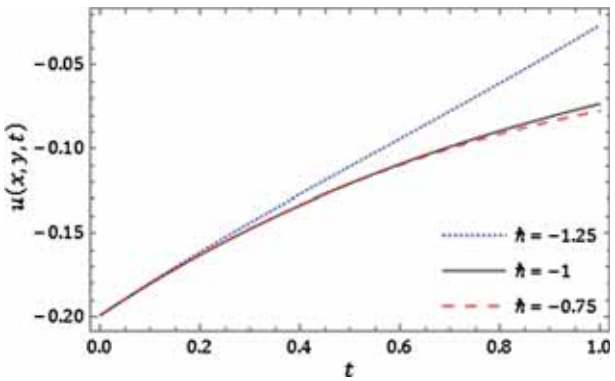

Figure 5. Plot of q-HATM solution $u(x, y, t)$ when $n = 1$, $\alpha = 1, g = 0, \rho_0 = 0.5$ and $x = 0.1 = y$ with diverse values of $\hbar$, for Example 1.

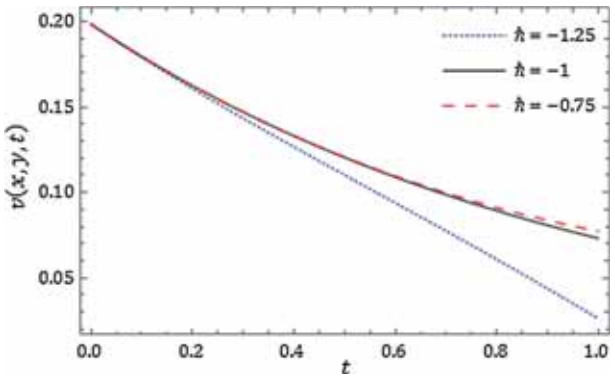

Figure 6. Plot of q-HATM solution $v(x, y, t)$ when $n = 1, \alpha = 1, g = 0, \rho_0 = 0.5$ and $x = 0.1 = y$ with diverse values of $\hbar$, for Example 1.

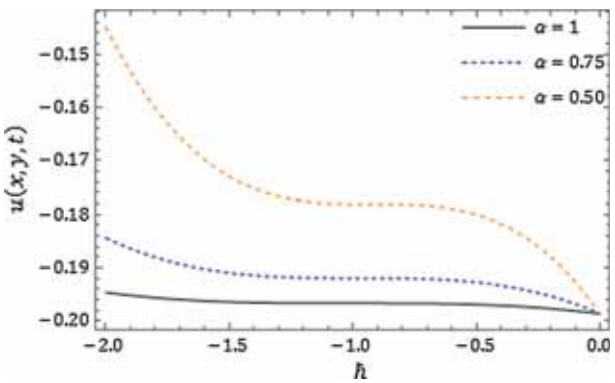

Figure 7. $\hbar$-Curves for q-HATM solution $u(x, y, t)$ when $g = 0, \rho_0 = 0.5, x = y = 0.1, t = 0.01$ and $n = 1$ with diverse values of α, for Example. 1.

$$v(x, y, t) = e^{x+y}\left[1 + \frac{2\rho_0 t}{1!} + \frac{(2\rho_0 t)^2}{2!} + \frac{(2\rho_0 t)^3}{3!} + \cdots\right] = e^{x+y+2\rho_0 t}.$$

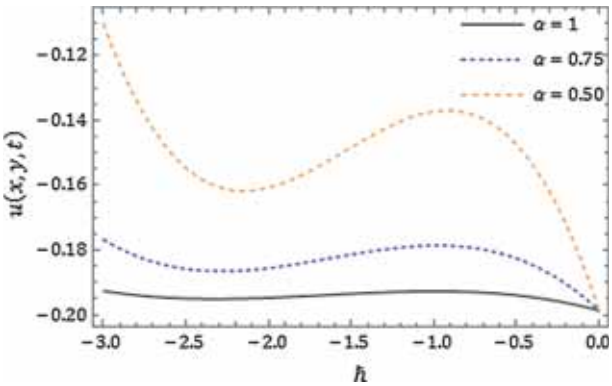

Figure 8. $\hbar$-Curves for q-HATM solution $u(x, y, t)$ when $g = 0, \rho_0 = 0.5, x = y = 0.1, t = 0.01$ and $n = 2$ with diverse values of α, for Example 1.

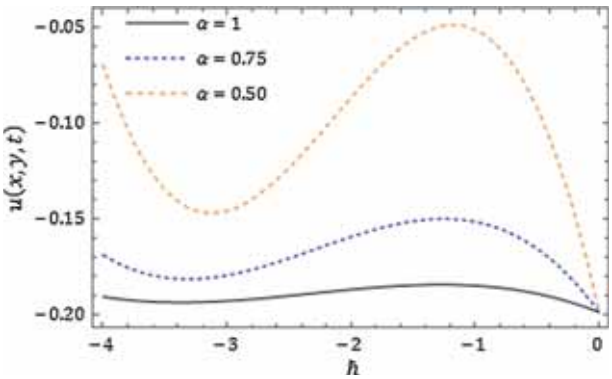

Figure 9. $\hbar$-Curves for q-HATM solution $u(x, y, t)$ when $g = 0, \rho_0 = 0.5, x = y = 0.1, t = 0.01$ and $n = 3$ with diverse values of α, for Example 1.

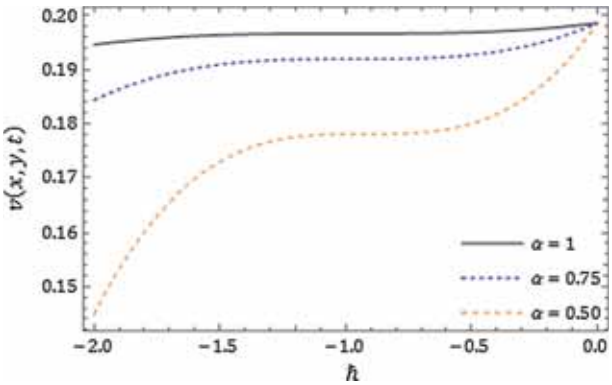

Figure 10. $\hbar$-Curves for q-HATM solution $v(x, y, t)$ when $g = 0, \rho_0 = 0.5, x = y = 0.1, t = 0.01$ and $n = 1$ with diverse values of α, for Example 1.

5. Numerical results and discussion

The efficiency of the proposed algorithm for Example 1 is presented in figures 1 and 2. Here, figures 1a, 1b and 2a, 2b show surfaces of fourth-order approximate

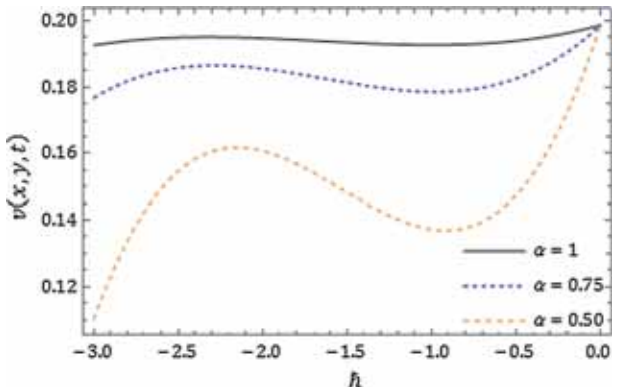

Figure 11. $\hbar$-Curves for q-HATM solution $v(x, y, t)$ when $g = 0, \rho_0 = 0.5, x = y = 0.1, t = 0.01$ and $n = 2$ with diverse values of α, for Example 1.

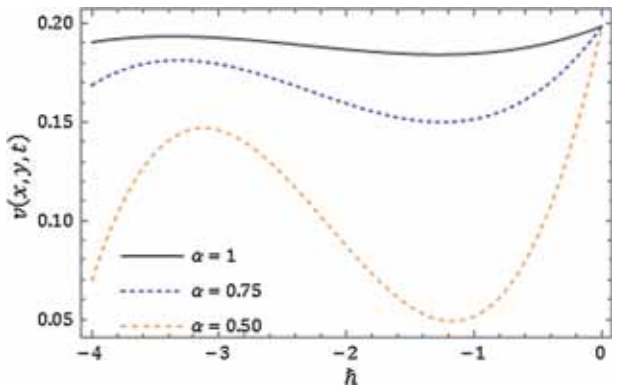

Figure 12. $\hbar$-Curves for q-HATM solution $v(x, y, t)$ when $g = 0, \rho_0 = 0.5, x = y = 0.1, t = 0.01$ and $n = 3$ with diverse values of α, for Example 1.

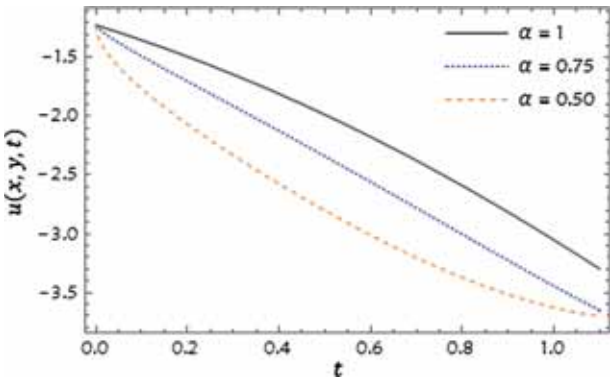

Figure 15. Plot of q-HATM solution $u(x, y, t)$ vs. t when $n = 1, \hbar = -1, g = 0, \rho_0 = 0.5$ and $x = 0.1 = y$ with diverse values of α, for Example 2.

and exact solutions for systems (18) and (19). Figures 1c and 2c show the competence of q-HATM through an absolute error. Figures 3 and 4 exhibit the behaviour of a numerical solution for diverse values of α at $n = 1$, $\hbar = -1, g = 0, \rho_0 = 0.5$ and $x = 0.1 = y$ for the system considered in Example 1. From figures 3 and 4, it is realised that the solution of the fractional-order system depends not only on time but also on the arbitrary order α. In figures 5 and 6, distinct values of $\hbar$ are chosen to lessen the error. Effects of asymptotic parameter n are shown in figures 7–12 for Example 1. Moreover, the effectiveness of q-HATM solution for Example 2 is presented in figures 13 and 14. Figures 13a, 13b and 14a, 14b show surfaces of fourth-order approximate and exact solutions for system (18) with conditions (27). Figures 13c and 14c reveal the efficiency of q-HATM through an absolute error. Figures 15 and 16 show the

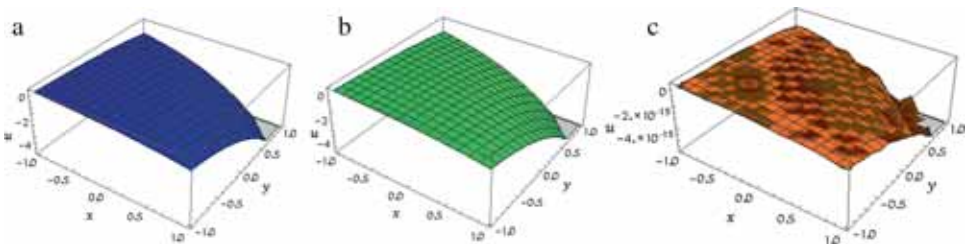

Figure 13. Surface of (**a**) approximate solution, (**b**) exact solution and (**c**) abs. error $= \left|u_{\text{exact}} - u_{\text{approx.}}\right|$ when $n = 1 = \alpha, \hbar = -1, g = 0, \rho_0 = 0.5$ and $t = 0.1$, for Example 2.

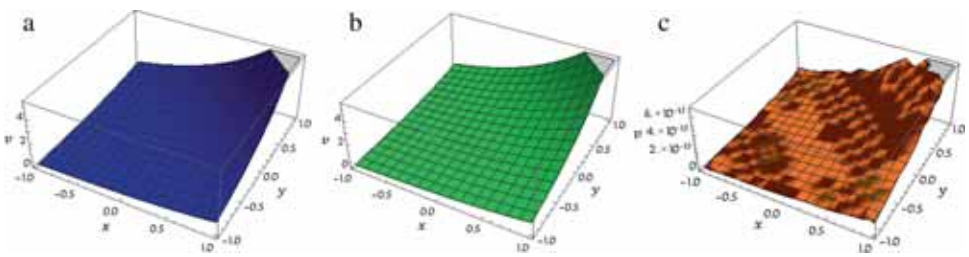

Figure 14. Surface of (**a**) approximate solution, (**b**) exact solution and (**c**) abs. error $= \left|v_{\text{exact}} - v_{\text{approx.}}\right|$ when $n = 1 = \alpha, \hbar = -1, g = 0, \rho_0 = 0.5$ and $t = 0.1$, for Example 2.

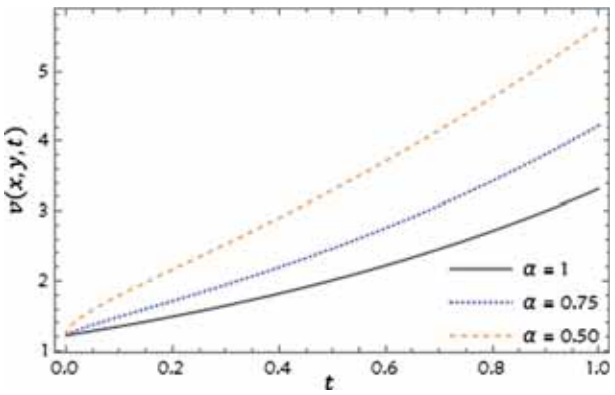

Figure 16. Plot of q-HATM solution $v(x, y, t)$ vs. t when $n = 1, \hbar = -1, g = 0, \rho_0 = 0.5$ and $x = 0.1 = y$ with diverse values of α, for Example 2.

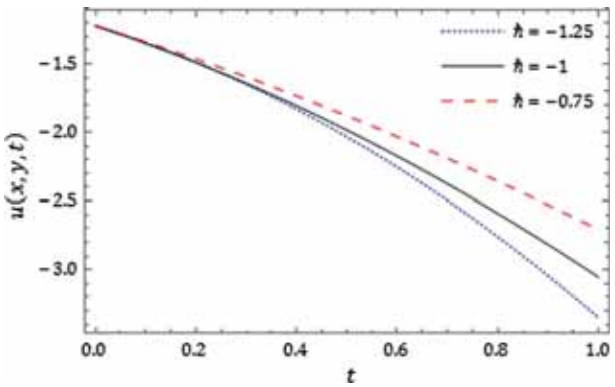

Figure 17. Plot of q-HATM solution $u(x, y, t)$ when $n = 1, \alpha = 1, g = 0, \rho_0 = 0.5$ and $x = 0.1 = y$ with diverse values of $\hbar$, for Example 2.

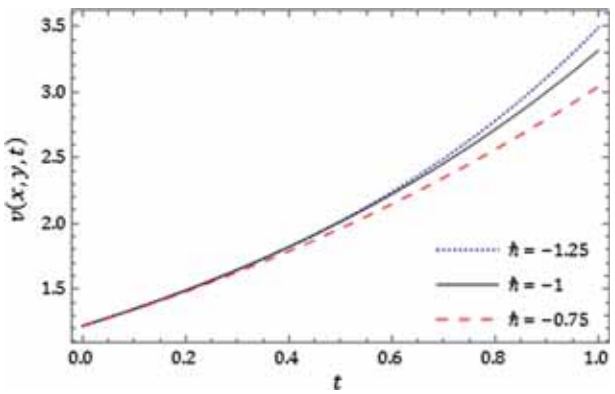

Figure 18. Plot of q-HATM solution $v(x, y, t)$ when $n = 1, \alpha = 1, g = 0, \rho_0 = 0.5$ and $x = 0.1 = y$ with diverse values of $\hbar$, for Example 2.

behaviour of numerical solution for diverse values of α at $n = 1, \hbar = -1, g = 0, \rho_0 = 0.5$ and $x = 0.1 = y$ for the system considered in Example 2. From figures 15 and 16, it is again found that the solution of fractional-order system depends not only on time but also on α. In figures 17 and 18, distinct values of $\hbar$ are preferred to lessen the residual error. Effects of asymptotic parameter n are shown in figures 19–24 for Example 2.

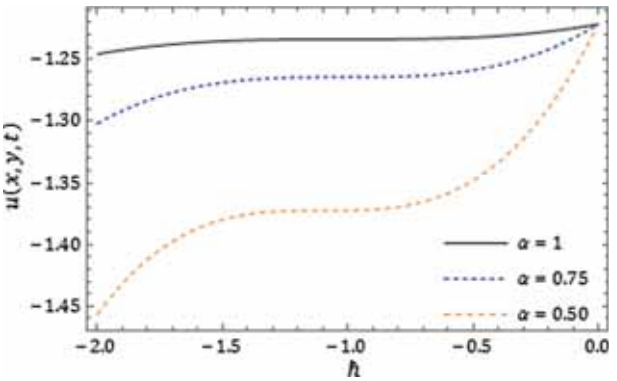

Figure 19. $\hbar$-Curves for q-HATM solution $u(x, y, t)$ when $g = 0, \rho_0 = 0.5, x = 0.1 = y, t = 0.01$ and $n = 1$ with diverse values of α, for Example 2.

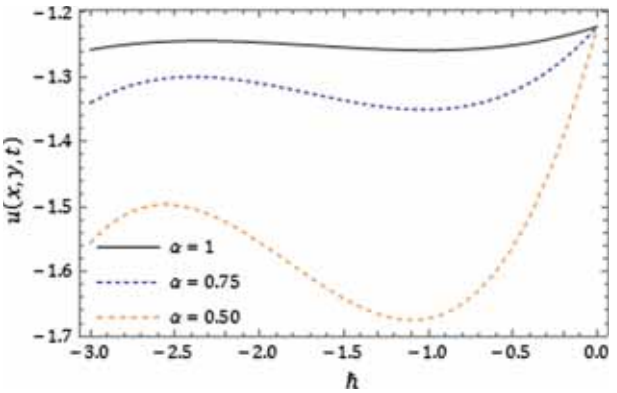

Figure 20. $\hbar$-Curves for q-HATM solution $u(x, y, t)$ when $g = 0, \rho_0 = 0.5, x = 0.1 = y, t = 0.01$ and $n = 2$ with diverse values of α, for Example 2.

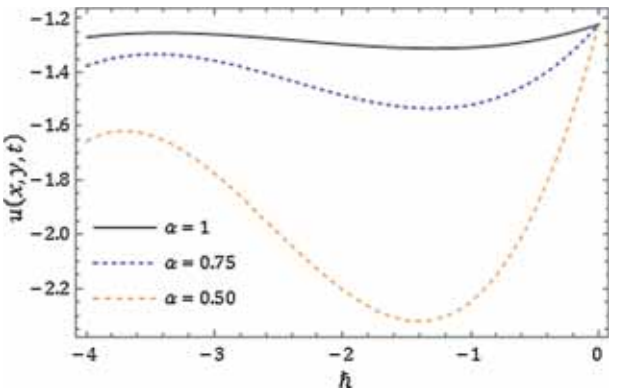

Figure 21. $\hbar$-Curves for $u(x, y, t)$ when $g = 0, \rho_0 = 0.5$, $x = 0.1 = y, t = 0.01$ and $n = 3$ with different α, for Example 2.

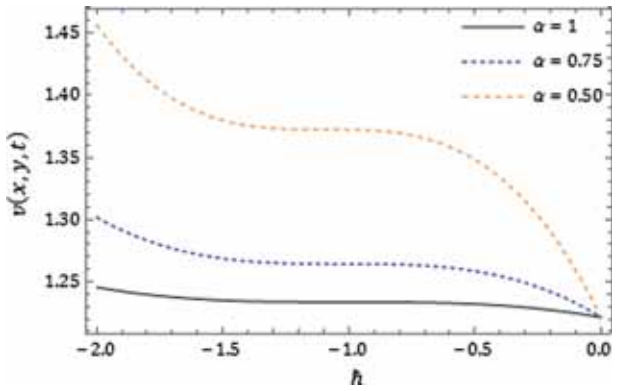

Figure 22. $\hbar$-Curves for $v(x, y, t)$ when $g = 0$, $\rho_0 = 0.5$, $x = 0.1 = y, t = 0.01$ and $n = 1$ with different α, for Example 2.

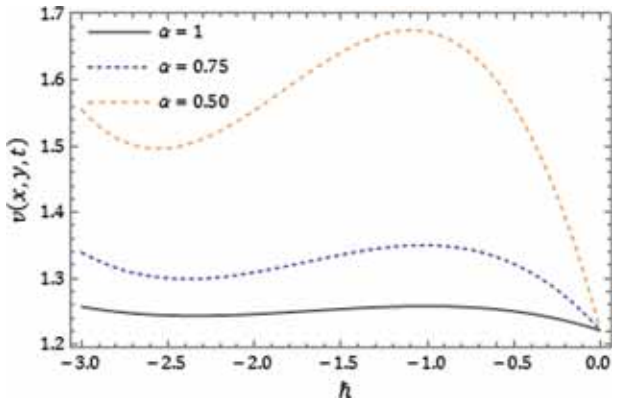

Figure 23. $\hbar$-Curves for q-HATM solution $v(x, y, t)$ when $g = 0, \rho_0 = 0.5, x = 0.1 = y, t = 0.01$ and $n = 2$ with diverse values of α, for Example 2.

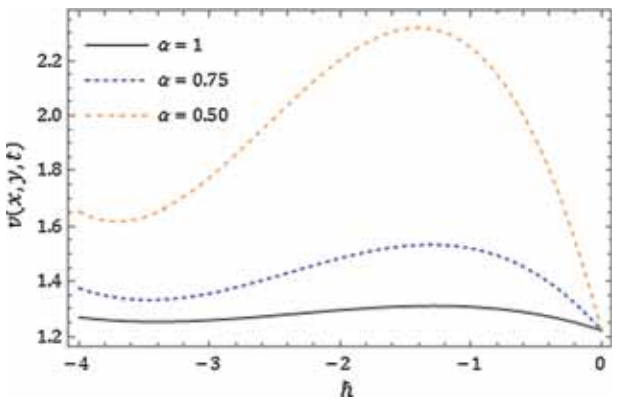

Figure 24. $\hbar$-Curves for q-HATM solution $v(x, y, t)$ when $g = 0, \rho_0 = 0.5, x = 0.1 = y, t = 0.01$ and $n = 3$ with diverse values of α, for Example 2.

6. Conclusions

In the present framework, q-HATM is successfully applied to find the numerical solution of coupled time-fractional NS equations. The obtained results demonstrate the reliability and simplicity of the method. The proposed algorithm provides parameter $\hbar$ that helps us to control the convergence region of series solution. As q-HATM does not necessitate linearisation, small perturbations or discretisation, it decreases computations significantly. In comparison with other techniques, q-HATM is a competent tool to get numerical solution of coupled nonlinear fractional partial differential equations (FPDEs).

Acknowledgements

The authors are thankful to the reviewers and the editor for their valuable suggestions and comments to improve the quality of the paper.

References

[1] J H He, *Int. J. Theor. Phys.* **53**(**11**), 3698 (2014)
[2] F J Liu, H Y Liu, Z B Li and J H He, *Therm. Sci.* **21**, 1867 (2017)
[3] J H He, *Results Phys.* **10**, 272 (2018)
[4] D Tripathi, *Acta Astonantaut.* **68**(**7–8**), 1379 (2011)
[5] V E Tarasov, *Ann. Phys.* **323**(**11**), 2756 (2008)
[6] M Mirzazadeh, *Pramana – J. Phys.* **86**(**5**), 957 (2016)
[7] I Podlubny, *Fractional differential equations* (Academic Press, New York, 1999)
[8] K S Miller and B Ross, *An introduction to fractional calculus and fractional differential equations* (Wiley-Blackwell, New York, 1993)
[9] A A Kilbas, H M Srivastava and J J Trujillo, *Theory and applications of fractional differential equations* (Elsevier, Amsterdam, 2006)
[10] A Prakash, M Goyal and S Gupta, *Nonlinear Eng.* **8**, 164 (2019), https://doi.org/10.1515/nleng-2018-0001
[11] A Prakash, M Goyal and S Gupta, *Pramana – J. Phys.* **92**: 18 (2019), https://doi.org/10.1007/s12043-018-1683-1
[12] M El-Shahed and A Salem, *Appl. Math. Comput.* **156**(**1**), 287 (2004)
[13] B K Singh and P Kumar, *Ain Shams Eng. J.* **9(4)**, 827 (2018), https://doi.org/10.1016/j.asej.2016.04.009
[14] G A Birajdar, *Nonlinear Eng.* **3**(**1**), 21 (2014)
[15] D Kumar, J Singh and S Kumar, *J. Assoc. Arab Univ. Basic Appl. Sci.* **17**, 14 (2015)
[16] S J Liao, *Appl. Math. Comput.* **147**(**2**), 499 (2004)
[17] A Prakash and H Kaur, *Chaos Solitons Fractals* **105**, 99 (2017)
[18] H M Srivastava, D Kumar and J Singh, *Appl. Math. Model.* **45**, 192 (2017)
[19] D Kumar, J Singh and D Baleanu, *Nonlinear Dyn.* **91**, 307 (2018)
[20] J Singh, D Kumar and R Swaroop, *Alexandria Eng. J.* **55**(**2**), 1753 (2016)